https://doi.org/10.5194/bg-2019-341
Preprint. Discussion started: 3 September 2019

Biogeosciences Discussions
Open Access
EGU

A numerical model study of the main factors contributing to hypoxia and its sub-seasonal to interannual variability off the Changjiang Estuary

Haiyan Zhang[1, 2], Katja Fennel[1,*], Arnaud Laurent[1], Changwei Bian[3]

[1]Department of Oceanography, Dalhousie University, Halifax, Nova Scotia, Canada
[2]School of Marine Science and Technology, Tianjin University, Tianjin, China
[3] Physical Oceanography Laboratory/CIMST, Ocean University of China, and Qingdao National Laboratory for Marine Science and Technology, Qingdao, China
*Corresponding author

Abstract

A three-dimensional physical-biological model of marginal seas of China was used to analyze variations in hypoxic conditions and identify the main processes controlling their generation off the Changjiang Estuary. The model was validated against available observations and reproduces the observed temporal and spatial variability of hypoxia. Dissolved oxygen concentrations undergo a seasonal cycle, with minima generally occurring in August or September, and vary latitudinally with a longer duration of low-oxygen concentrations in the southern part of the hypoxic region. Interannual variations of hypoxic extent are primarily associated with variations in river discharge and wind forcing, with high river discharge promoting hypoxia generation. At synoptic time scales, strong wind events (e.g. typhoons) can disrupt hypoxic conditions. During the oxygen-depleted period (March-August), air-sea exchange acts as an oxygen sink in oversaturated surface waters. In the subsurface, biological oxygen consumption tends to dominate, but lateral physical transport of oxygen can be comparable during hypoxic conditions. Oxygen consumption in the water column exceeds that of the sediment when integrated over the whole water column, but sediment consumption is dominant below the pycnocline. Vertical diffusion of oxygen acts as the primary oxygen source below the pycnocline and shows a seasonal cycle similar to that of primary production. Advection of oxygen in the bottom waters acts as an oxygen sink in spring but becomes a source during hypoxic conditions in

https://doi.org/10.5194/bg-2019-341
Preprint. Discussion started: 3 September 2019

summer especially in the southern part of the hypoxic region, which is influenced by open-ocean intrusions.

1. Introduction

In coastal seas, hypoxic conditions (oxygen concentrations lower than 2 mg L^{-1} or 62.5 mmol m^{-3}) are increasingly caused by rising anthropogenic nutrient loads from land (Diaz & Rosenberg, 2008; Rabalais et al., 2010; Fennel and Testa, 2019). Hypoxic conditions are detrimental to coastal ecosystems leading to a decrease in species diversity and rendering these systems less resilient (Baird et al., 2004; Bishop et al., 2006; Wu, 2002). Hypoxia is especially prevalent in coastal systems influenced by major rivers such as the northern Gulf of Mexico (Bianchi et al., 2010), Chesapeake Bay (Li et al., 2016), and the Changjiang Estuary (CE) in the East China Sea (Li et al., 2002).

The Changjiang River is the largest river in China and fifth largest in the world in terms of volume transport, with an annual discharge of 9×10^{11} m^3 $year^{-1}$ via its estuary (Liu et al., 2003). The mouth of the CE is at the confluence of the southeastward Yellow Sea Coastal Current and the northward Taiwan Warm Current (TWC; Figure 1). Hydrographic properties in the outflow region of the CE are influenced by several different water masses including fresh Changjiang Diluted Water (CDW), relatively low-salinity coastal water, more saline TWC water and high-nutrient, low-oxygen water from the subsurface of the Kuroshio (Wei et al., 2015; Yuan et al., 2008). The interactions of these water masses together with wind forcing and tidal effects lead to a complicated and dynamic environment.

Freshwater discharge reaches the minimum in winter when the strong northerly monsoon (dry season) prevails and peaks in summer during the weak southerly monsoon (wet season) resulting in a large river plume adjacent to the estuary. Along with the freshwater, the Changjiang River delivers large quantities of nutrients to the East China Sea (ECS) and the Yellow Sea (YS) resulting in eutrophication in the plume region (Li et al., 2014; Wang et al., 2016). Since the 1970s, nutrient load has increased more than twofold with a subsequent increase in primary production in the outflow region of the estuary (Liu et al., 2015). Hypoxia off the CE was first detected in 1959 and, with a spatial extent of up to 15,000 km^2, is among the largest coastal hypoxic zones in the world (Fennel & Testa 2019). Although no conclusive trend in oxygen minima has been observed (Wang, 2009; Zhu et

https://doi.org/10.5194/bg-2019-341
Preprint. Discussion started: 3 September 2019

al., 2011), hypoxic conditions are suspected to have expanded and intensified in recent decades (Li et al., 2011; Ning et al., 2011) due to the increasing nutrient loads from the Changjiang River (Liu et al., 2015).

It is generally accepted that water-column stratification and the decomposition of organic matter are the two essential factors for hypoxia generation and this is also the case for the shelf region off the CE (Chen et al., 2007; Li et al., 2002; Wei et al., 2007). High solar radiation and freshwater input in summer contribute to strong vertical stratification which is further enhanced by near-bottom advection of TWC waters with high salinities (> 34) and low temperatures (< 19 °C). This strong stratification inhibits vertical oxygen supply (Li et al., 2002; Wang, 2009; Wei et al., 2007). At the same time, high organic matter supply fuels microbial oxygen consumption in the subsurface (Li et al., 2002; Wang, 2009; Wei et al., 2007; Zhu et al., 2011). It has also been suggested that the TWC brings additional nutrients contributing to organic matter production (Ning et al., 2011) and that the low oxygen concentrations (~ 5 mg L^{-1}) of the TWC precondition the region to hypoxia (Ning et al., 2011; Wang, 2009).

While observational analyses suggest that hypoxia off the CE results from the interaction of various physical and biogeochemical processes, quantifying the relative importance of these processes and revealing the dynamic mechanisms underlying hypoxia development and variability require numerical modeling (Peña et al., 2010). Numerical modeling studies have proven useful for many other coastal hypoxic regions such as the Black Sea northwestern shelf (Capet et al., 2013), Chesapeake Bay (Li et al., 2016; Scully, 2013), and the northern Gulf of Mexico (Fennel et al., 2013; Laurent & Fennel, 2014).

Models have also been used to study the hypoxic region of the CE. Chen et al. (2015a) used a 3D circulation model with a highly simplified oxygen consumption parameterization (a constant consumption rate) to investigate the effects of physical processes, i.e. freshwater discharge, and wind speed and direction, on hypoxia formation. Chen et al. (2015b) examined the tidal modulation of hypoxia. The model domain in these two previous studies was relatively limited encompassing only the CE, Hangzhou Bay and the adjacent coastal ocean but did not cover the whole area affected by hypoxia (Wang, 2009; Zhu et al., 2011). Zheng et al. (2016) employed a nitrogen cycle model coupled with a 3D hydrodynamic model to examine the role of river discharge, wind speed and direction on

https://doi.org/10.5194/bg-2019-341
Preprint. Discussion started: 3 September 2019

hypoxia, and also emphasized the physical controls. These previous modeling studies focused on the response of hypoxia to physical factors only and did not address seasonal evolution and interannual variations of hypoxia.

More recently, Zhou et al. (2017) analyzed the seasonal evolution of hypoxia and the importance of TWC and Kuroshio intrusions as a nutrient source using an advanced coupled hydrodynamic-biological model. However, the baseline of their model does not include sediment oxygen consumption (SOC), which is thought to be a major oxygen sink in the hypoxic region off the CE (Zhang et al., 2017) and other river-dominated hypoxic regions including the northern Gulf of Mexico (Fennel et al. 2013, Yu et al. 2015a,b). Zhou et al. (2017) acknowledged the importance of SOC based on results from a sensitivity experiment but did not quantify its role in hypoxia generation.

Here we introduce a new 3D physical-biological model implementation for the ECS that explicitly includes nitrogen and phosphorus cycling and SOC. The model is a new regional implementation for the ECS of an existing physical-biogeochemical model framework that has been extensively used and validated for the northern Gulf of Mexico (Fennel et al., 2011, 2013; Laurent et al., 2012; Laurent and Fennel, 2014; Yu et al., 2015b; Fennel and Laurent, 2018). The hypoxic zones in northern Gulf of Mexico and off the CE have similar features including the dominant influence of a major river (Changjiang and Mississippi), a seasonal recurrence every summer, a typical maximum size of about 15,000 km^2, documented P-limitation following the major annual discharge in spring and a significant contribution of SOC to oxygen sinks in the hypoxic zone (Fennel and Testa 2019). Here the model is used to explore the evolution of hypoxia on subseasonal to interannual scales and to identify the main factors contributing to the different modes of variability. For this study, we performed and validated a 6-year simulation in the ECS, discuss the main drivers of short-term to interannual variability, and present an oxygen budget to quantify the relative importance of SOC and the influence of lateral advection of oxygen.

2. Model description

2.1. Physical model

The physical model used in this study is based the Regional Ocean Modeling System (ROMS; Haidvogel et al., 2008) and was implemented for the ECS by Bian et al. (2013a).

https://doi.org/10.5194/bg-2019-341
Preprint. Discussion started: 3 September 2019

The model domain extends from 116°E to 134°E and from 20°N to 42°N (Figure 1), covering the Bohai Sea (BS), the YS, the ECS, part of the Japan Sea and the adjacent northwest Pacific, with a horizontal resolution of 1/12° and 30 vertical layers with enhanced resolution near the surface and bottom. The model uses the recursive Multidimensional Positive Definite Advection Transport Algorithm (MPDATA) for the advection of tracers, a third-order upstream advection of momentum, and the Generic Length Scale (GLS) turbulence closure scheme (Umlauf & Burchard, 2003) for vertical mixing.

The model is initialized with climatological temperature and salinity from the World Ocean Atlas 2013 V2 (WOA13 V2) (Locarnini et al., 2013; Zweng et al., 2013), and is forced by 6-hourly wind stress, and heat and freshwater fluxes from the ECMWF ERA-Interim dataset (Dee et al., 2011). Open boundary conditions for temperature and salinity are prescribed from the monthly climatology (WOA13 V2), and horizontal velocities and sea surface elevation at the boundaries are specified from the SODA data set (Carton & Giese, 2008). In addition, eight tidal constituents (M2, S2, N2, K2, K1, O1, P1 and Q1) are imposed based on tidal elevations and currents are extracted from the global inverse tide model data set of TPXO7.2 of Oregon State University (OSU, Egbert & Erofeeva, 2002). At the open boundaries, Chapman and Flather conditions are used for the free surface and the barotropic velocity, respectively, and the radiation condition for the baroclinic velocity. Eleven rivers are included in the model. Freshwater discharge from the Changjiang River uses daily observations from the Datong Hydrological Station (DHS; www.cjh.com.cn) while the other rivers are prescribed from monthly or annual climatologies (Liu et al., 2009; Tong et al., 2015; Zhang, 1996).

https://doi.org/10.5194/bg-2019-341
Preprint. Discussion started: 3 September 2019

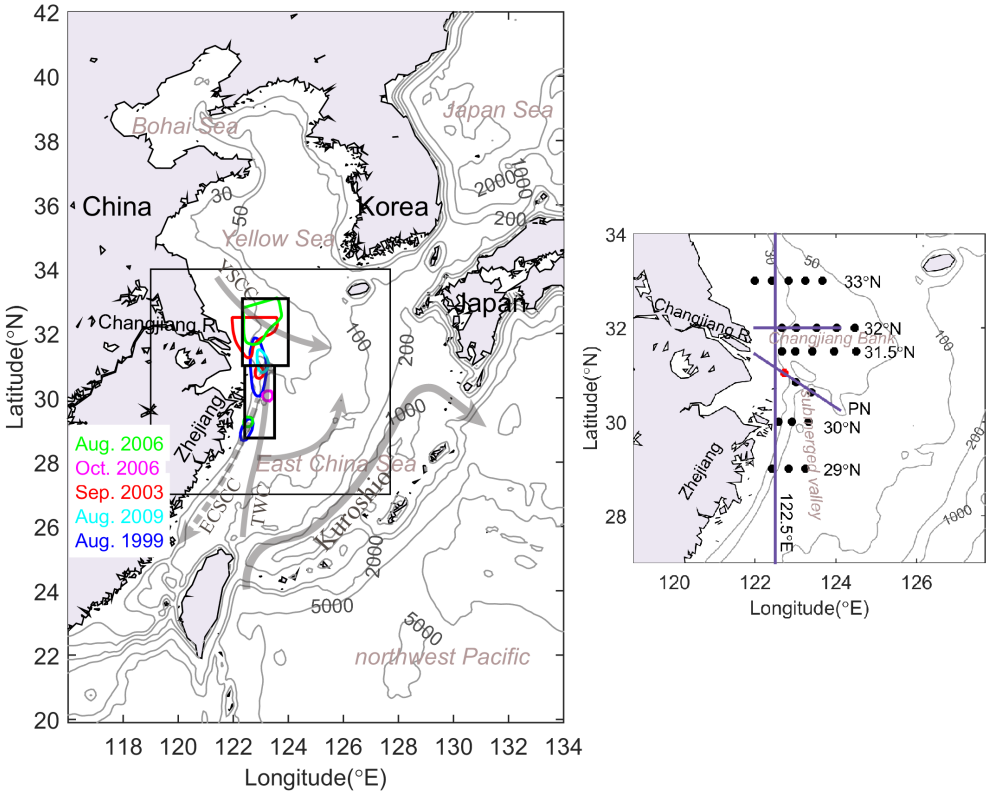

Figure 1. (left panel) Bathymetry of the model domain with isobaths (in meters). Colored polygons near the CE indicate observed hypoxic extent in previous studies (Li et al., 2002; Wei et al., 2007; Zhou et al., 2010; Zhu et al., 2016). Two small black boxes indicate the northern and southern regions used in the analysis. Solid grey arrows denote currents present throughout the year (Kuroshio; TWC: Taiwan Warm Current; YSCC: Yellow Sea Coastal Current). The dashed grey arrow indicates the direction of the wintertime current where flows are in the opposite direction in summertime (ECSCC: East China Sea Coastal Current). The larger black box indicates the location of the subregion magnified in the right panel. (right panel) Three solid lines indicate transects (32°N, 122.5°E, PN) used in Figure 6.

2.2. Biological model

The biological component is based on the pelagic nitrogen cycle model of Fennel et al. (2006, 2011, 2013) and was extended to include phosphate (Laurent et al., 2012; Laurent & Fennel, 2014) and riverine dissolved organic matter (Yu et al., 2015b). The model includes two forms of dissolved inorganic nitrogen (DIN), nitrate (NO3) and ammonium

https://doi.org/10.5194/bg-2019-341
Preprint. Discussion started: 3 September 2019

(NH4), phosphate (PO4), phytoplankton (Phy), chlorophyll (Chl), zooplankton (Zoo), two pools of detritus, suspended and slow-sinking small detritus (SDet) and fast-sinking large detritus (LDet), and riverine dissolved organic matter (RDOM). Here, riverine dissolved and particulate organic nitrogen enter the pools of RDOM and SDet, respectively. The remineralization rate of RDOM is an order of magnitude lower than that of SDet to account for the more refractory nature of the riverine dissolved organic matter (Yu et al., 2015b).

At the sediment-water interface, SOC is parameterized assuming "instantaneous remineralization," i.e. all organic matter reaching the sediment is remineralized instantaneously and oxygen is consumed due to nitrification and aerobic remineralization at the same time. In the "instantaneous remineralization", all phosphorus is returned to the water column as PO4 while a constant fraction of fixed nitrogen is lost due to denitrification. All biogeochemical model parameters are given in Table S1 in the Supplement. A more detailed model descriptions can be found in the Supplement to Laurent et al. (2017).

To account for light attenuation due to colored dissolved organic matter (CDOM) and suspended sediments, which show relatively high values near the coast and in the river plume (Bian et al., 2013b; Chen et al., 2014), a light-attenuation term dependent on water depth and salinity is introduced which yields higher attenuation in shallower and fresher areas.

Initial and boundary conditions for NO3, PO4 and oxygen are prescribed using the World Ocean Atlas 2013 (WOA13) climatology (Garcia et al., 2013a,b). A small positive value is used for the other variables. NO3 is nudged towards climatology in the northwest Pacific at depth > 200 m. Monthly nutrient loads of DIN and PO4 from the Changjiang River are from the Global-NEWs Model (Wang et al., 2015). Nutrient loads in other rivers are based other published climatologies (Liu et al., 2009; Tong et al., 2015; Zhang, 1996).

We performed an 8-year simulation from 1 January 2006 to 31 December 2013, with 2006-2007 as model spin up and 2008-2013 used for analysis. Two geographical regions, the northern hypoxic region and the southern hypoxic region, are defined for analysis near the CE (Figure 1). The northern region corresponds to the Changjiang Bank and the southern region represents the submerged valley and Zhejiang coastal area.

3. Results

https://doi.org/10.5194/bg-2019-341
Preprint. Discussion started: 3 September 2019

195 **3.1. Simulated oxygen dynamics**

196 First, we compare simulated and observed oxygen distributions in near-bottom waters
197 for 9 cruises between March 2011 and September 2013 (Figure 2). The model and
198 observations agree well for the first 5 cruises in 2011 and 2012, but the simulated hypoxic
199 area is smaller and less severe than observed in June, July and August 2013. Nevertheless,
200 the model agrees well with the observed seasonal evolution and spatial distribution of
201 observed bottom oxygen with an overall correlation coefficient of 0.76. Further validation
202 of simulated surface and bottom distributions of temperature and salinity, a comparison of
203 surface chlorophyll against satellite observations, and an assessment of the seasonal
204 variations and transports of the major currents compared to observation-based estimates
205 (Hu et al., 2010; Guo et al. 2005; Takikawa and Yoon, 2005; Fukudome et al., 2010) are
206 presented in the Supplement. Together, these comparisons show that the model is able to

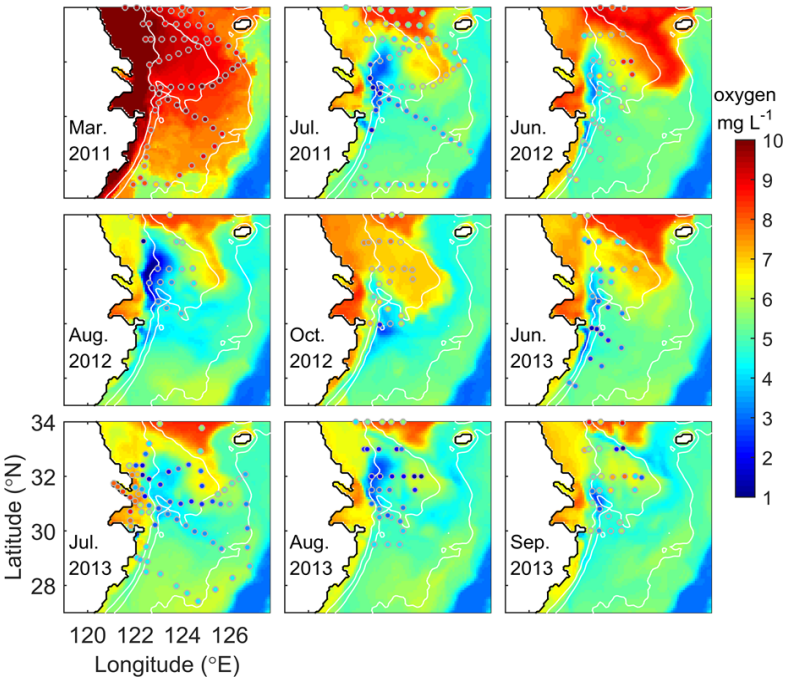

Figure 2. Simulated bottom oxygen (colored map) compared with observations (dots) during nine cruises from 2011 to 2013.

207 reproduce important aspects of the physical-biogeochemical dynamics in general and the
208 spatio-temporal evolution of oxygen in bottom waters in particular.

https://doi.org/10.5194/bg-2019-341
Preprint. Discussion started: 3 September 2019

209 In aggregate, Figure 2 suggests a typical seasonal cycle of hypoxia development with
210 well-oxygenated bottom waters in March, hypoxic conditions establishing in June and July,
211 becoming most pronounced in August, and beginning to disperse in September. However,
212 the model simulates significant interannual variability in timing and extent of hypoxia over
213 the 6-year simulation period from 2008 to 2013 (Figure 3a). The years with largest
214 maximum hypoxic extent are 2010 (13,800 km^2), 2009 (13,700 km^2), 2008 (12,000 km^2)
215 and 2012 (11,500 km^2) while the simulated hypoxic extent is much smaller (<4,000 km^2)
216 in 2011 and 2013. The ranking is similar when considering the time-integrated hypoxic
217 extent (Figure 3b). The year with the largest maximum and integrated hypoxic extent
218 (2010) also has the highest peak discharge (Figure 3a) and highest annual freshwater
219 discharge (65,400 $m^3 s^{-1}$), although the annual discharge is similar to 2008 and 2012. Since
220 freshwater discharge and nutrient load are strongly related (Figure 3b), it is obvious that
221 severe hypoxia is simulated in the years with large freshwater discharge and nutrient load.

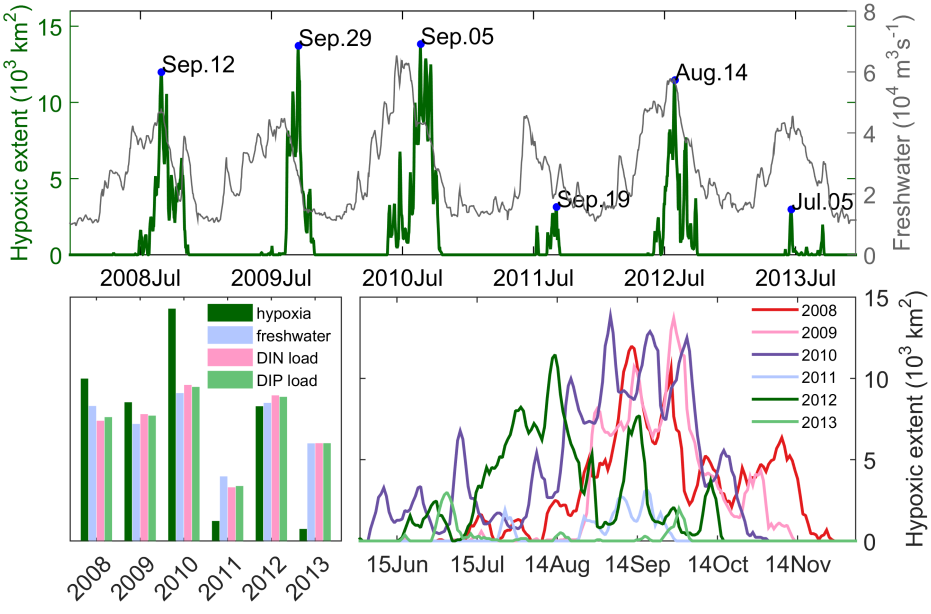

Figure 3. Time series of freshwater discharge and simulated hypoxic extent with peaks specified by date (a). Normalized annual time-integrated hypoxic extent, freshwater discharge, and DIN and DIP load (b). Evolution of simulated hypoxic extent by year (c).

https://doi.org/10.5194/bg-2019-341
Preprint. Discussion started: 3 September 2019

There are marked differences in the phenology of simulated hypoxic extent (Figure 3c). Among the four years with largest hypoxic areas, hypoxia establishes relatively late (mid-August) and lasts long (into November) in 2008 and 2009. In contrast in 2012, hypoxic conditions establish earlier (June), are most pronounced in August and are eroded by mid-October. In 2010, the year with the largest peak extent, hypoxia establishes already at the beginning of June and is maintained until the end of October, leading to the by far largest time-integrated hypoxia among the 6 years (Figure 3b). In all years there are short periods during which the hypoxic extent decreases rapidly. These decreases are due to wind events eroding vertical stratification and thus leading to resupply of oxygen over short time scales (days), as illustrated for 2012 in Figure 4. The year 2012 saw the passage of four typhoons (Haikui, Bolaven, Sanba and Prapiroon). Coincident with the passage of Haikui, Bolaven and Sanba (indicated by spikes in windstress), hypoxic area decreased, especially for Bolaven and Sanba. Prapiroon passed after hypoxia had eroded completely and thus had no effect (Figure 4a). Even moderate spikes in windstress (e.g., a week before Haikui and half-way between Sanba and Prapiroon) can lead to decreases in hypoxia extent. Panels 4b

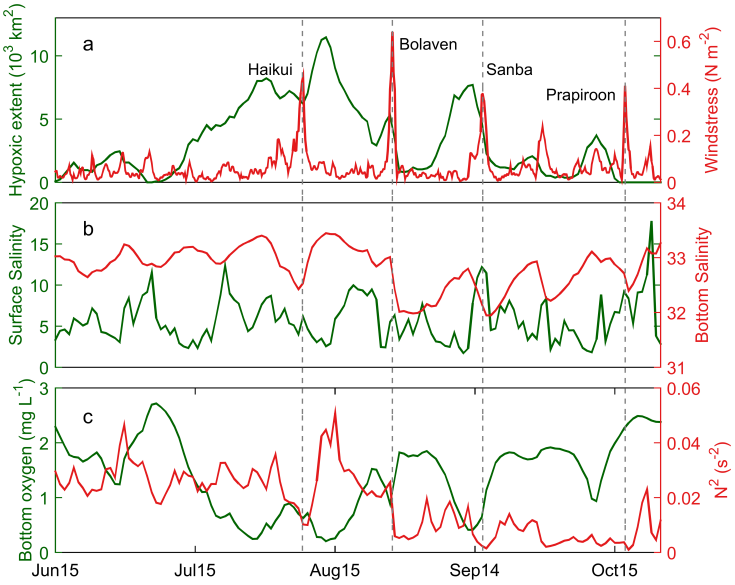

Figure 4. Evolution of hypoxic area and space-averaged wind stress (a), minimum surface salinity and space-averaged bottom salinity (b), minimum bottom oxygen and space-averaged N^2 (c) in 2012. Dashed vertical lines indicate when typhoons passed over hypoxic region.

https://doi.org/10.5194/bg-2019-341
Preprint. Discussion started: 3 September 2019

and c show that wind events lead to freshening of bottom water salinity, decreases in stratification strength (measured by N^2) and increases in bottom-water oxygen. However, not every decrease in hypoxic area is linked to a wind event; see, e.g., the slow decrease during the calm 2nd half of August where bottom salinity and stratification strength are decreasing and bottom-water oxygen increasing more slowly.

Spatial distributions of bottom oxygen and surface salinity for the same year are shown in Figure 5 and illustrate their complex spatial patterns. Hypoxia appears first near the Zhejiang coast and further north in June and strengthens in July. In early August, hypoxia expands northward onto Changjiang Bank, while weakening and then disappearing near the Zhejiang coast. After reaching its peak extent on August 13, hypoxia starts to disperse in the northern regions and reappears further south near the Zhejiang coast in September. This spatial expression of hypoxia is mirrored in the spatial distribution of Changjiang Diluted Water (CDW), which generally extends southeastward or eastward in spring, veers northeastward in summer and then southeastward again in autumn relative to the mouth of the estuary (Figure 5). The patterns are similar in other years.

Vertical distributions of temperature, salinity, oxygen and nutrients during hypoxic conditions are shown in Figure 6 to illustrate the spatial structure in the north-south, east-west and inshore-offshore directions. The north-south transect at 122.5°E shows relatively cold (< 20°C) and salty (> 34) bottom water with relatively high nitrate (> 5 μmol L^{-1}) and phosphate (~1 μmol L^{-1}) concentrations climbing inshore from the south and southeast. Bottom hypoxia occurs within this cold bottom water below the CDW (surface salinity < 28). The Yellow Sea Cold Water Mass (YSCWM), characterized by temperature less than 10°C, marks the northern boundary of hypoxic water. The cross-shore transects (32°N and PN) illustrate the offshore extension of the thin surface layer of CDW, its associated high nitrate concentrations, and the underlying hypoxic water. The thickness of the hypoxic layer ranges from a few meters to over 20 m.

https://doi.org/10.5194/bg-2019-341
Preprint. Discussion started: 3 September 2019

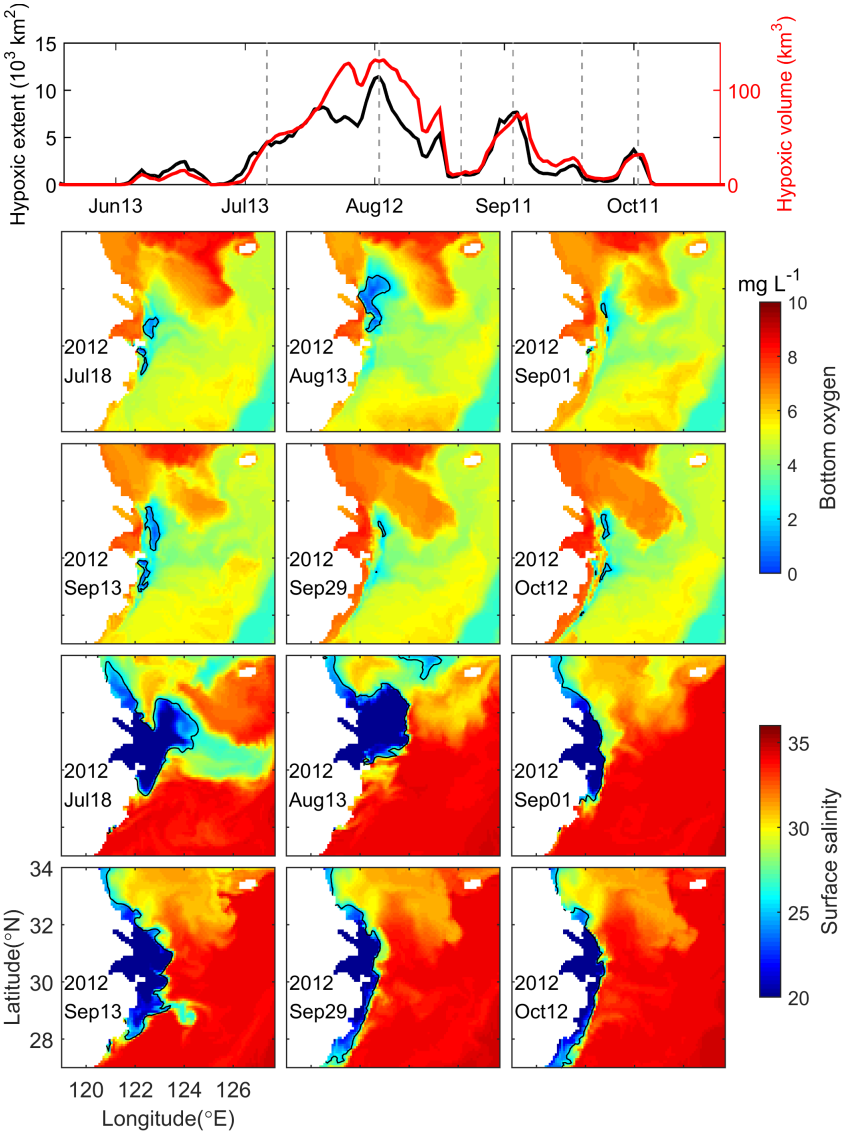

Figure 5. Time series of hypoxic extent and volume in 2012 (top panel), bottom oxygen (middle two rows) and surface salinity (bottom two rows) distributions at different times in 2012, which are indicated by the vertical lines in the top panel. The contour in oxygen panels denotes the isoline of 2 mg L^{-1}. The contour in salinity panels denotes the isoline of 26.

263

264

https://doi.org/10.5194/bg-2019-341
Preprint. Discussion started: 3 September 2019

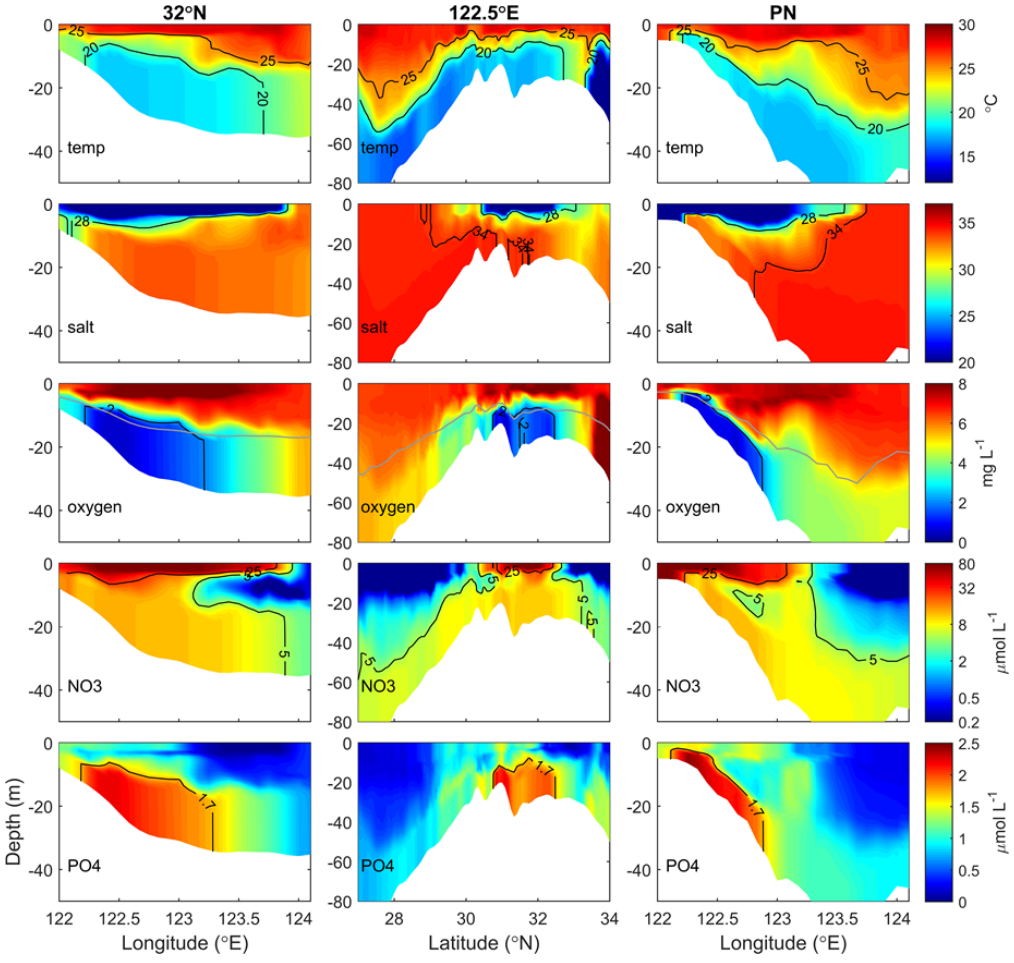

Figure 6. Temperature, salinity, oxygen, NO3 and PO4 distribution at transects along 32°N, 122.5°E and transect PN (Figure 1) on August 13, 2012 when hypoxia is severe, with isolines indicated by black lines. Grey lines in oxygen distribution maps denote the border below which is bottom waters for oxygen budget in the following section.

265

266 **3.2 Oxygen budgets for the northern and southern regions**

267 In order to identify the roles of key physical and biological processes in regulating
268 hypoxia, an oxygen budget is calculated for the period from March to August for the
269 northern and southern hypoxic regions. Considering that hypoxic conditions occur near the
270 bottom, we evaluate an oxygen budget not only for the whole water column but also for its

https://doi.org/10.5194/bg-2019-341
Preprint. Discussion started: 3 September 2019

lower portion that typically becomes hypoxic. To account for variations in the thickness of the hypoxic layer, which tends to be thicker in deeper waters (also indicated by observations in Ning et al., 2011), we include the bottommost 12 layers of our model grid. Because of the model's terrain-following vertical coordinates, the thickness of these 12 model layers varies with total depth as shown by the gray lines in the oxygen panels in Figure 6. The terms considered in the budget are air-sea flux, lateral physical advection and diffusion, vertical turbulent diffusion (for the subsurface budget only), photosynthetic production, water-column oxygen consumption (i.e., respiration and nitrification), and SOC. Each term is integrated vertically over the whole water column and also over the bottom-most 12 layers and then averaged for the northern and southern regions for each month (Figure 7, Table S2 in the Supplement).

For the whole water column (Figure 7 a, b), biological processes (PP, WR and SOC) greatly exceed physical processes (air-sea exchange and advective transport) in affecting oxygen. PP is always greater than the sum of WR and SOC in the whole column indicating autotrophy in spring and summer. Advection is negative, acting as an oxygen sink and offsetting 10%-17% and 8%-27% of PP in the northern and southern regions, respectively. Of the two biological oxygen consumption terms (WR and SOC), WR accounts for 54%-57% and 56%-58% in the northern and southern regions, respectively, slightly larger than SOC. Negative air-sea flux indicates oxygen outgassing into the atmosphere, which is associated with photosynthetic oxygen production and decreasing oxygen solubility due to

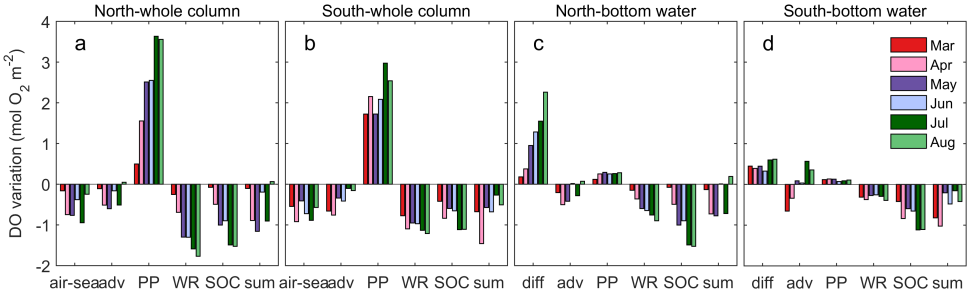

Figure 7. Monthly averaged (2008-2013) oxygen budgets for the whole water column and subsurface water from March to August in the northern and southern hypoxic regions (refer to Figure 1). Adv represents lateral advection (and lateral diffusion which is comparatively small). Diff represents vertical turbulent diffusion, which is only relevant for the subsurface budget.

https://doi.org/10.5194/bg-2019-341
Preprint. Discussion started: 3 September 2019

increasing temperature. However, since hypoxia only occurs in the subsurface, the subsurface budget below is more instructive.

When considering only subsurface waters (Figure 7 c, d), the influence of PP decreases markedly, accounting for only 4%-11% of that in the whole water column. Vertical turbulent diffusion acts as the largest oxygen source in the subsurface layer. SOC is the dominant oxygen sink accounting for 61%-63% and 69%-73% of the total biological oxygen consumption in the northern and southern regions, respectively. As photosynthetic oxygen production strengthens gradually from spring to summer (see Figure 7 a, b) WR and SOC also increase as they are closely associated with photosynthetically-produced organic matter. Vertical oxygen diffusion tends to covary with PP, implying an oxygen gradient driven by photosynthetic oxygen production in the upper layer. Lateral advection of oxygen is negative in the early months of the hypoxic season (March, April) in both regions, but becomes positive later (July, August) in the southern region. This suggests that early in the hypoxic season, import of low-oxygen water contributes to hypoxia generation in both regions but switches to an oxygen source later in the southern region. Overall, oxygen sources and sink terms are similar in the northern and southern regions, except for turbulent diffusion from the upper layer into the subsurface which is much greater in the northern region.

4. Discussion

The model simulates hypoxia in subsurface waters off the CE with two core centers: the southern region near the Zhejiang coast and in the submerged valley northeast of Zhejiang, and the northern region centered on Changjiang Bank. These model results are consistent with observed hypoxia locations (Li et al., 2002; Wei et al., 2007; Zhu et al., 2016, 2011). The simulated seasonal cycle of hypoxic conditions, developing first in the southern region, strengthening northward to reach their maximum extent between August and September, and then retreating southward, also agrees with the available observations (Wang et al., 2012; Zhu et al., 2011) albeit limited. The subseasonal north-south shifts in hypoxia location match shifts in the surface distribution of CDW, underscoring the important role of density stratification in facilitating hypoxic conditions. Relative to the CE mouth, the CDW generally extends southeastward in spring, veers northeastward to Cheju Island in

https://doi.org/10.5194/bg-2019-341
Preprint. Discussion started: 3 September 2019

summer and then again southeast in autumn, due to the Asian monsoon. The hypoxic layer is found below the main pycnocline and can be more than 20 m thick in August, in agreement with observations (Li et al., 2002; Ning et al., 2011).

Hypoxic extent exhibits pronounced interannual and subseasonal variability. Years with more severe hypoxia are also years with high river discharge and large associated nutrient loads, suggesting that these are the major factors controlling interannual variation of hypoxia off the CE. This is consistent with previous studies (Zheng et al., 2016; Zhou et al., 2017). In addition, the model simulates large variations in hypoxic extent on short time scales (days). Large and rapid decreases in hypoxic extent result from wind events, including typhoons, and can disrupt hypoxia multiple times throughout the same hypoxic season (as shown for 2012). Hypoxic conditions tend to be restored within a few days after typhoon passage; a phenomenon that has been documented by time series observations in the region (Ni et al., 2016; Wang et al. 2017).

Oxygen budgets for the northern and southern regions typically encompassing the hypoxic zones provide valuable insights into the importance of surface and subsurface processes, the dominant role of SOC in the subsurface and the contribution of horizontal advection of oxygen to regional and seasonal hypoxia dynamics. When considering the whole water column, which is always autotrophic in these regions, biological processes greatly exceed lateral transport of oxygen. Lateral oxygen transport always acts as a sink. And WR accounts for more than half of the biological oxygen consumption (SOC is the smaller contributor). However, when considering the subsurface only (here the bottom-most 12 layers of the model grid), a different picture emerges. In the subsurface, the largest oxygen source is vertical turbulent diffusion (PP is insignificant). Lateral transport is a more important term, compared to the whole water column budget, and acts sometimes as sink and other times as source. The latter is most obvious in July and August in the southern region and indicates that lateral advection contributes to mitigation of hypoxia in the southern region toward the end of the hypoxic season. And SOC is the dominant oxygen sink in the subsurface.

This comparison between whole-water column and subsurface-only budgets emphasizes the importance of considering the latter, providing insights into when and where lateral advection amplifies or mitigates hypoxia and that SOC is the dominant oxygen sink in the

https://doi.org/10.5194/bg-2019-341
Preprint. Discussion started: 3 September 2019

353 subsurface. The relative importance of WR and SOC had not previously been quantified
354 for this region due to lack of concurrent WR and SOC observations and lack of models that
355 realistically account for both processes. The budget for the whole water column is
356 dominated by the oxygen sources, sinks and transport in the surface layer, which does not
357 experience hypoxia.
358 The importance of SOC in our model is consistent with recent observational studies.
359 SOC on the coastal shelves in the YS and ECS has been estimated to range from 1.7 to 17.6
360 mmol O_2 m^{-2} d^{-1} (mean rate of 7.2 mmol O_2 m^{-2} d^{-1}) from April to October except August
361 by Song et al. (2016), and from 9.1 to 62.5 mmol O_2 m^{-2} d^{-1} (mean of 22.6±16.4 mmol O_2
362 m^{-2} d^{-1}) from June to October in Zhang et al. (2017). Simulated SOC falls within the
363 observed range with a mean rate of 13.5±11.5 mmol O_2 m^{-2} d^{-1} between April and October.
364 Based on observations, Zhang et al. (2017) already suggested that SOC is a major
365 contributor to hypoxia formation in below-pycnocline waters, which further corroborated
366 by our model results. It is also consistent with the modelling study of Zhou et al. (2017),
367 who did not include SOC in the baseline version of their model but showed in a sensitivity
368 study that inclusion of SOC simulates hypoxic extent more realistically. Our results are in
369 line with findings from the northern Gulf of Mexico hypoxic zone where WR is much
370 larger than SOC below the pycnocline, while SOC is dominant in the bottom 5 m where
371 hypoxia occurs most frequently in summer (Quiñones-Rivera et al., 2007; Yu et al., 2015b).
372 The finding that lateral oxygen transport can act as a net source to subsurface water is
373 also new. On seasonal scales, oxygen advection in the subsurface varies from an oxygen
374 sink in spring to a source in summer, especially in the southern hypoxic region, implying
375 that the TWC becomes an oxygen source when oxygen is depleted in the hypoxic region.
376 This aspect was neglected in previous studies which only emphasized the role of advection
377 as an oxygen sink promoting hypoxia formation (Ning et al., 2011; Qian et al., 2015). The
378 TWC originates from the subsurface of the Kuroshio northeast to Taiwan Island, and thus
379 represents an intrusion onto the continental shelves from the open ocean (Guo et al., 2006).
380 In addition to oxygen advection, nutrients are transported supporting primary production
381 on the ECS shelves (Zhao & Guo, 2011). The intrusion of the TWC and the Kuroshio
382 accompanied by relatively cold and saline water, and nutrient and oxygen transport, is
383 thought to influence hypoxia development (Li et al., 2002; Wang, 2009; Zhou et al., 2017)

https://doi.org/10.5194/bg-2019-341
Preprint. Discussion started: 3 September 2019

but no quantification of the relative importance has occurred until now (see companion paper by Grosse et al. using the same model).

5. Conclusions

In this study, a new 3D coupled physical-biological model for the ECS was presented and used to explore the spatial and temporal evolution of hypoxia off the CE and to quantify the major processes controlling oxygen dynamics. Validation shows that the model reproduces the observed spatial distribution and temporal evolution of physical and biological variables well. Overall, simulated hypoxia generally occurs near the Zhejiang coast and the submerged valley to its east (the southern hypoxic region) and on the Changjiang Bank (the northern region) and is dominated by behavior of the CDW and local wind-driven current system. Simulated hypoxia duration is generally longer in the southern hypoxic region.

Pronounced interannual variations of hypoxic extent in our 6-year simulation are primarily associated with differences in river discharge and nutrient load as larger freshwater and nutrient inputs enhance water column stratification and primary production, respectively, and thus are conducive to hypoxia development. On synoptic time scales, strong wind events (e.g. typhoons) can disrupt simulated hypoxia significantly, but only for short periods.

A model-derived oxygen budget shows that SOC is larger than WR in the subsurface of the hypoxic region. Lateral oxygen advection in the subsurface switches from an oxygen sink in spring to a source in summer especially in the southern hypoxic region and is likely associated with the TWC supplying open-ocean intrusions onto the coastal shelf.

Acknowledgments

This work was supported by the National Key Research and Development Program of China (2016YFC1401602 and 2017YFC1404403). The authors thank the crew of the Dongfanghong2 for providing much help during the sampling cruises, and Compute Canada for access to supercomputer time. Financial support to HZ from the China Scholarship Council (CSC) is gratefully acknowledged. KF also acknowledges support from the NSERC Discovery Program. The model forcing datasets (WOA, ECMWF, SODA,

TPXO7.2) used in this study are publicly available and related papers are cited in the reference list. Websites of the satellite data (SST, chlorophyll) and the Changjiang freshwater data have been given where they are used. Nutrients data of rivers are available in published papers cited in the reference list. The model results are available on request to the authors.

References

Baird, D., Christian, R. R., Peterson, C. H., & Johnson, G. A.: Consequences of hypoxia on estuarine ecosystem function: Energy diversion from consumers to microbes. Ecological Applications, 14(3), 805–822. https://doi.org/10.1890/02-5094, 2004.

Bian, C., Jiang, W., & Greatbatch, R. J.: An exploratory model study of sediment transport sources and deposits in the Bohai Sea, Yellow Sea, and East China Sea. Journal of Geophysical Research: Oceans, 118(11), 5908–5923. https://doi.org/10.1002/2013JC009116, 2013a.

Bian, C., Jiang, W., Quan, Q., Wang, T., Greatbatch, R. J., & Li, W.: Distributions of suspended sediment concentration in the Yellow Sea and the East China Sea based on field surveys during the four seasons of 2011. Journal of Marine Systems, *121–122*, 24–35, https://doi.org/10.1016/j.jmarsys.2013.03.013, 2013b.

Bianchi, T. S., DiMarco, S. F., Cowan, J. H., Hetland, R. D., Chapman, P., Day, J. W., & Allison, M. A.: The science of hypoxia in the northern Gulf of Mexico: A review. Science of the Total Environment, 408(7), 1471–1484. https://doi.org/10.1016/j.scitotenv.2009.11.047, 2010.

Bishop, M. J., Powers, S. P., Porter, H. J., & Peterson, C. H.: Benthic biological effects of seasonal hypoxia in a eutrophic estuary predate rapid coastal development. Estuarine, Coastal and Shelf Science, 70(3), 415–422. https://doi.org/10.1016/j.ecss.2006.06.031, 2006.

Capet, A., Beckers, J. M., & Grégoire, M.: Drivers, mechanisms and long-term variability of seasonal hypoxia on the Black Sea northwestern shelf - Is there any recovery after eutrophication? Biogeosciences, 10(6), 3943–3962. https://doi.org/10.5194/bg-10-3943-2013, 2013.

Carton, J. A., & Giese, B. S.: A Reanalysis of Ocean Climate Using Simple Ocean Data Assimilation (SODA). Monthly Weather Review, 136(8), 2999–3017, https://doi.org/10.1175/2007MWR1978.1, 2008.

Chen, C. C., Gong, G. C., & Shiah, F. K., Hypoxia in the East China Sea: One of the largest coastal low-oxygen areas in the world. Marine Environmental Research, 64(4), 399–408. https://doi.org/10.1016/j.marenvres.2007.01.007, 2007.

448 Chen, J., Cui, T., Ishizaka, J., & Lin, C.: A neural network model for remote sensing of diffuse
449 attenuation coefficient in global oceanic and coastal waters: Exemplifying the applicability of
450 the model to the coastal regions in Eastern China Seas. Remote Sensing of Environment, *148*,
451 168–177. https://doi.org/10.1016/j.rse.2014.02.019, 2014.
452 Chen, X., Shen, Z., Li, Y., & Yang, Y.: Physical controls of hypoxia in waters adjacent to the
453 Yangtze Estuary: A numerical modeling study. Marine Pollution Bulletin, *97*(1–2), 349–364.
454 https://doi.org/10.1016/j.marpolbul.2015.05.067, 2015a.
455 Chen, X., Shen, Z., Li, Y., & Yang, Y.: Tidal modulation of the hypoxia adjacent to the Yangtze
456 Estuary in summer. Marine Pollution Bulletin, *100*(1), 453–463,
457 https://doi.org/10.1016/j.marpolbul.2015.08.005, 2015b.
458 Dee, D. P., Uppala, S. M., Simmons, A. J., Berrisford, P., Poli, P., Kobayashi, S., … Vitart, F.:
459 The ERA-Interim reanalysis: Configuration and performance of the data assimilation system.
460 Quarterly Journal of the Royal Meteorological Society, *137*(656), 553–597.
461 https://doi.org/10.1002/qj.828, 2011.
462 Diaz, R. J., & Rosenberg, R.: Spreading dead zones and consequences for marine ecosystems.
463 Science, *321*(5891), 926–929. https://doi.org/10.1126/science.1156401, 2008.
464 Egbert, G. D., & Erofeeva, S. Y.: Efficient inverse modeling of barotropic ocean tides. Journal of
465 Atmospheric and Oceanic Technology, *19*(2), 183–204. https://doi.org/10.1175/1520-
466 0426(2002)019<0183:EIMOBO>2.0.CO;2, 2002.
467 Fennel, K., and Testa, J.M.: Biogeochemical controls on coastal hypoxia, Annual Review of
468 Marine Science, 11, 105-130, https://doi.org/10.1146/annurev-marine-010318-095138, 2019.
469 Fennel, K. and Laurent, A.: N and P as ultimate and proximate limiting nutrients in the northern
470 Gulf of Mexico: implications for hypoxia reduction strategies, Biogeosciences, 15, 3121-3131,
471 https://doi.org/ /10.5194/bg-15-3121-2018, 2018.
472 Fennel, K., Hetland, R., Feng, Y., & DiMarco, S.: A coupled physical-biological model of the
473 Northern Gulf of Mexico shelf: Model description, validation and analysis of phytoplankton
474 variability. Biogeosciences, *8*(7), 1881–1899. https://doi.org/10.5194/bg-8-1881-2011, 2011.
475 Fennel, K., Hu, J., Laurent, A., Marta-Almeida, M., & Hetland, R.: Sensitivity of hypoxia
476 predictions for the northern Gulf of Mexico to sediment oxygen consumption and model
477 nesting. Journal of Geophysical Research: Oceans, *118*(2), 990–1002.
478 https://doi.org/10.1002/jgrc.20077, 2013.
479 Fennel, K., Wilkin, J., Levin, J., Moisan, J., O'Reilly, J., & Haidvogel, D.: Nitrogen cycling in
480 the Middle Atlantic Bight: Results from a three-dimensional model and implications for the

https://doi.org/10.5194/bg-2019-341
Preprint. Discussion started: 3 September 2019

North Atlantic nitrogen budget. Global Biogeochemical Cycles, *20*(3), 1–14. https://doi.org/10.1029/2005GB002456, 2006.

Fukudome, K.-I., Yoon, J.-H., Ostrovskii, A., Takikawa, T., & Han, I.-S.: Seasonal volume transport variation in the Tsushima warm current through the Tsushima Straits from 10 years of ADCP observations, Journal of Oceanography, 66, 539-551, 2010.

Garcia, H. E., Boyer, T. P., Locarnini, R. A., Antonov, J. I., Mishonov, A. V, Baranova, O. K., … Johnson, D. R.: World Ocean Atlas 2013. Volume 3: dissolved oxygen, apparent oxygen utilization, and oxygen saturation. NOAA Atlas NESDIS 75, 2013a.

Garcia, H. E., Locarnini, R. A., Boyer, T. P., Antonov, J. I., Baranova, O. K., Zweng, M. M., … Johnson, D. R.: World Ocean Atlas 2013, Volume 4 : Dissolved Inorganic Nutrients (phosphate, nitrate, silicate). NOAA Atlas NESDIS 76 (Vol. 4), 2013b.

Grosse, F., Fennel, K., Zhang, H., Laurent, A.: Quantifying the contributions of riverine vs. oceanic nitrogen to hypoxia in the East China Sea, (submitted to same Biogeosciences Special Issue; ms bg-2019-342)

Guo, J. S., X. M. Hu and Y. L. Yuan: A diagnostic analysis of variations in volume transport through the Taiwan Strait using satellite altimeter data, Advances in Marine Science, 23(1): 20 – 26 (in Chinese with English abstract), 2005.

Guo, X., Miyazawa, Y., & Yamagata, T.: The Kuroshio Onshore Intrusion along the Shelf Break of the East China Sea: The Origin of the Tsushima Warm Current. Journal of Physical Oceanography, 36(12), 2205–2231. https://doi.org/10.1175/JPO2976.1, 2006.

Haidvogel, D. B., Arango, H., Budgell, W. P., Cornuelle, B. D., Curchitser, E., Di Lorenzo, E., … Wilkin, J., Ocean forecasting in terrain-following coordinates: Formulation and skill assessment of the Regional Ocean Modeling System. Journal of Computational Physics, 227(7), 3595–3624. https://doi.org/10.1016/j.jcp.2007.06.016, 2008.

Hu, J., Kawamura, H., Li, C., Hong, H., Jiang, Y.: Review on current and seawater volume transport through the Taiwan Strait, Journal of Oceanography, 66, 591-610, 2010.

Laurent, A., & Fennel, K.: Simulated reduction of hypoxia in the northern Gulf of Mexico due to phosphorus limitation. Elementa: Science of the Anthropocene, *2*(1), 000022. https://doi.org/10.12952/journal.elementa.000022, 2014.

Laurent, A., Fennel, K., Hu, J., & Hetland, R.: Simulating the effects of phosphorus limitation in the Mississippi and Atchafalaya river plumes. Biogeosciences, *9*(11), 4707–4723. https://doi.org/10.5194/bg-9-4707-2012, 2012.

Laurent, A., Fennel, K., Cai, W.-J., Huang, W.-J., Barbero, L., Wanninkhof, R.: Eutrophication-Induced Acidification of Coastal Waters in the Northern Gulf of Mexico: Insights into Origin

and Processes from a Coupled Physical-Biogeochemical Model. Geophys. Res. Lett., *44* (2), 946–956. https://doi.org/10.1002/2016GL071881, 2012.

Li, D., Zhang, J., Huang, D., Wu, Y., & Liang, J.: Oxygen depletion off the Changjiang (Yangtze River) Estuary. Science in China Series D: Earth Science, *45*(12), 1137. https://doi.org/10.1360/02yd9110, 2002.

Li, H. M., Tang, H. J., Shi, X. Y., Zhang, C. S., & Wang, X. L.: Increased nutrient loads from the Changjiang (Yangtze) River have led to increased Harmful Algal Blooms. Harmful Algae, *39*, 92–101. https://doi.org/10.1016/j.hal.2014.07.002, 2014.

Li, M., Lee, Y. J., Testa, J. M., Li, Y., Ni, W., Kemp, W. M., & Di Toro, D. M.: What drives interannual variability of hypoxia in Chesapeake Bay: Climate forcing versus nutrient loading? Geophysical Research Letters, *43*(5), 2127–2134. https://doi.org/10.1002/2015GL067334, 2016.

Li, X., Bianchi, T. S., Yang, Z., Osterman, L. E., Allison, M. A., DiMarco, S. F., & Yang, G.: Historical trends of hypoxia in Changjiang River estuary: Applications of chemical biomarkers and microfossils. Journal of Marine Systems, *86*(3–4), 57–68, 2011. https://doi.org/10.1016/j.jmarsys.2011.02.003

Liu, K. K., Yan, W., Lee, H. J., Chao, S. Y., Gong, G. C., & Yeh, T. Y.: Impacts of increasing dissolved inorganic nitrogen discharged from Changjiang on primary production and seafloor oxygen demand in the East China Sea from 1970 to 2002. *Journal of Marine Systems*, *141*, 200–217. https://doi.org/10.1016/j.jmarsys.2014.07.022, 2015.

Liu, S. M., Hong, G.-H., Ye, X. W., Zhang, J., & Jiang, X. L.: Nutrient budgets for large Chinese estuaries and embayment. Biogeosciences Discussions, *6*(1), 391–435. https://doi.org/10.5194/bgd-6-391-2009, 2009.

Liu, S. M., Zhang, J., Chen, H. T., Wu, Y., Xiong, H., & Zhang, Z. F.: Nutrients in the Changjiang and its tributaries. Biogeochemistry, *62*(1), 1–18, 2003.

Locarnini, R. A., Mishonov, A. V., Antonov, J. I., Boyer, T. P., Garcia, H. E., Baranova, O. K., … Seidov, D.: World Ocean Atlas 2013. Vol. 1: Temperature. S. Levitus, Ed.; A. Mishonov, Technical Ed.; NOAA Atlas NESDIS, 73, 40. https://doi.org/10.1182/blood-2011-06-357442, 2013.

Ni, X., Huang, D., Zeng, D., Zhang, T., Li, H., & Chen, J.: The impact of wind mixing on the variation of bottom dissolved oxygen off the Changjiang Estuary during summer. Journal of Marine Systems, 154, 122–130. https://doi.org/10.1016/j.jmarsys.2014.11.010, 2016.

547 Ning, X., Lin, C., Su, J., Liu, C., Hao, Q., & Le, F.: Long-term changes of dissolved oxygen,
548 hypoxia, and the responses of the ecosystems in the East China Sea from 1975 to 1995. Journal
549 of Oceanography, 67(1), 59–75. https://doi.org/10.1007/s10872-011-0006-7, 2011.
550 Peña, A., Katsev, S., Oguz, T., & Gilbert, D.: Modeling dissolved oxygen dynamics and hypoxia.
551 Biogeosciences, *7*(3), 933–957. https://doi.org/10.5194/bg-7-933-2010, 2010.
552 Qian, W., Dai, M., Xu, M., Kao, S. ji, Du, C., Liu, J., … Wang, L.: Non-local drivers of the
553 summer hypoxia in the East China Sea off the Changjiang Estuary. Estuarine, Coastal and
554 Shelf Science, 1–7. https://doi.org/10.1016/j.ecss.2016.08.032, 2015.
555 Quiñones-Rivera, Z. J., Wissel, B., Justić, D., & Fry, B.: Partitioning oxygen sources and sinks in
556 a stratified, eutrophic coastal ecosystem using stable oxygen isotopes. Marine Ecology
557 Progress Series, *342*, 69–83. https://doi.org/10.3354/meps342069, 2007.
558 Rabalais, N. N., Díaz, R. J., Levin, L. A., Turner, R. E., Gilbert, D., & Zhang, J.: Dynamics and
559 distribution of natural and human-caused hypoxia. Biogeosciences, *7*, 585–619.
560 https://doi.org/10.5194/bg-7-585-2010, 2010.
561 Scully, M. E.: Physical controls on hypoxia in Chesapeake Bay: A numerical modeling study.
562 Journal of Geophysical Research: Oceans, *118*(3), 1239–1256,
563 https://doi.org/10.1002/jgrc.20138, 2013.
564 Song, G., Liu, S., Zhu, Z., Zhai, W., Zhu, C., & Zhang, J.: Sediment oxygen consumption and
565 benthic organic carbon mineralization on the continental shelves of the East China Sea and the
566 Yellow Sea. Deep-Sea Research Part II: Topical Studies in Oceanography, *124*, 53–63.
567 https://doi.org/10.1016/j.dsr2.2015.04.012, 2016.
568 Takikawa, T., &Yoon, J.-H.: Volume transport through the Tsushima Straits estimated from Sea
569 level difference, Journal of Oceanography, 61, 699-708, 2005.
570 Tong, Y., Zhao, Y., Zhen, G., Chi, J., Liu, X., Lu, Y., … Zhang, W.: Nutrient Loads Flowing into
571 Coastal Waters from the Main Rivers of China (2006–2012). Scientific Reports, *5*, 16678.
572 https://doi.org/10.1038/srep16678, 2015.
573 Umlauf, L., & Burchard, H.: A generic length-scale equation for geophysical. Journal of Marine
574 Research, *61*(2), 235–265. https://doi.org/10.1357/002224003322005087, 2003.
575 Wang, B.: Hydromorphological mechanisms leading to hypoxia off the Changjiang estuary.
576 Marine Environmental Research, 67(1), 53–58,
577 https://doi.org/10.1016/j.marenvres.2008.11.001, 2009.
578 Wang, B., Wei, Q., Chen, J., & Xie, L.: Annual cycle of hypoxia off the Changjiang (Yangtze
579 River) Estuary. Marine Environmental Research, *77*, 1–5,
580 https://doi.org/10.1016/j.marenvres.2011.12.007, 2012.

581 Wang, B., Chen, J., Jin, H., Li, H., Huang, D., & Cai, W.-J.: Diatom bloom-derived bottom water
582 hypoxia off the Changjiang Estuary, with and without typhoon influence, Limnology and
583 Oceanography, 62, 1552-1569, https://doi.org/10.1002/lno.10517, 2017.
584 Wang, H., Dai, M., Liu, J., Kao, S. J., Zhang, C., Cai, W. J., … Sun, Z.: Eutrophication-Driven
585 Hypoxia in the East China Sea off the Changjiang Estuary. Environmental Science and
586 Technology, 50(5), 2255–2263. https://doi.org/10.1021/acs.est.5b06211, 2016.
587 Wang, J., Yan, W., Chen, N., Li, X., & Liu, L.: Modeled long-term changes of DIN:DIP ratio in
588 the Changjiang River in relation to Chl-α and DO concentrations in adjacent estuary. Estuarine,
589 Coastal and Shelf Science, *166*, 153–160. https://doi.org/10.1016/j.ecss.2014.11.028, 2015.
590 Wei, H., He, Y., Li, Q., Liu, Z., & Wang, H.: Summer hypoxia adjacent to the Changjiang
591 Estuary. Journal of Marine Systems, 67(3–4), 292–303,
592 https://doi.org/10.1016/j.jmarsys.2006.04.014, 2007.
593 Wei, H., Luo, X., Zhao, Y., & Zhao, L.: Intraseasonal variation in the salinity of the Yellow and
594 East China Seas in the summers of 2011, 2012, and 2013. Hydrobiologia, *754*(1), 13–28.
595 https://doi.org/10.1007/s10750-014-2133-9, 2015.
596 Wu, R. S. S.: Hypoxia: From molecular responses to ecosystem responses. Marine Pollution
597 Bulletin, *45*(1–12), 35–45. https://doi.org/10.1016/S0025-326X(02)00061-9, 2002.
598 Yu, L., Fennel, K., & Laurent, A.: A modeling study of physical controls on hypoxia generation
599 in the northern Gulf of Mexico. Journal of Geophysical Research C: Oceans, *120*(7), 5019–
600 5039. https://doi.org/10.1002/2014JC010634, 2015a.
601 Yu, L., Fennel, K., Laurent, A., Murrell, M. C., & Lehrter, J. C.: Numerical analysis of the
602 primary processes controlling oxygen dynamics on the Louisiana shelf. Biogeosciences, *12*(7),
603 2063–2076. https://doi.org/10.5194/bg-12-2063-2015, 2015b.
604 Yuan, D., Zhu, J., Li, C., & Hu, D.: Cross-shelf circulation in the Yellow and East China Seas
605 indicated by MODIS satellite observations. Journal of Marine Systems, *70*(1–2), 134–149.
606 https://doi.org/10.1016/j.jmarsys.2007.04.002, 2008.
607 Zhang, H., Zhao, L., Sun, Y., Wang, J., & Wei, H.: Contribution of sediment oxygen demand to
608 hypoxia development off the Changjiang Estuary. Estuarine, Coastal and Shelf Science, 192,
609 149–157. https://doi.org/10.1016/j.ecss.2017.05.006, 2017.
610 Zhang, J.: Nutrient elements in large Chinese estuaries. Continental Shelf Research, *16*(8), 1023–
611 1045. https://doi.org/10.1016/0278-4343(95)00055-0, 1996.
612 Zhao, L., & Guo, X.: Influence of cross-shelf water transport on nutrients and phytoplankton in
613 the East China Sea: A model study. Ocean Science, *7*(1), 27–43. https://doi.org/10.5194/os-7-
614 27-2011, 2011.

https://doi.org/10.5194/bg-2019-341
Preprint. Discussion started: 3 September 2019

615 Zheng, J., Gao, S., Liu, G., Wang, H., & Zhu, X.: Modeling the impact of river discharge and
616 wind on the hypoxia off Yangtze Estuary. Natural Hazards and Earth System Sciences, 16(12),
617 2559–2576. https://doi.org/10.5194/nhess-16-2559-2016, 2016.
618 Zhou, F., Chai, F., Huang, D., Xue, H., Chen, J., Xiu, P., … Wang, K.: Investigation of hypoxia
619 off the Changjiang Estuary using a coupled model of ROMS-CoSiNE. Progress in
620 Oceanography, 159, 237–254. https://doi.org/10.1016/j.pocean.2017.10.008, 2017.
621 Zhou, F., Huang, D., Ni, X., Xuan, J., Zhang, J., & Zhu, K.: Hydrographic analysis on the multi-
622 time scale variability of hypoxia adjacent to the Changjiang River Estuary. Shengtai Xuebao/
623 Acta Ecologica Sinica, 30(17), 4728–4740, 2010.
624 Zhu, J., Zhu, Z., Lin, J., Wu, H., & Zhang, J.: Distribution of hypoxia and pycnocline off the
625 Changjiang Estuary, China. Journal of Marine Systems, *154*, 28–40.
626 https://doi.org/10.1016/j.jmarsys.2015.05.002, 2016.
627 Zhu, Z.-Y., Zhang, J., Wu, Y., Zhang, Y.-Y., Lin, J., & Liu, S.-M.: Hypoxia off the Changjiang
628 (Yangtze River) Estuary: Oxygen depletion and organic matter decomposition. *Marine*
629 *Chemistry*, *125*(1–4), 108–116. https://doi.org/10.1016/j.marchem.2011.03.005, 2011.
630 Zweng, M. M., Reagan, J. R., Antonov, J. I., Mishonov, A. V., Boyer, T. P., Garcia, H. E., …
631 Bidlle, M. M., World Ocean Atlas 2013, Volume 2: Salinity. NOAA Atlas NESDIS (Vol. 119).
632 https://doi.org/10.1182/blood-2011-06-357442, 2013.
633